



This is a repository copy of *A generalized asymptotic extraction solution for antennas in multilayered spherical media*.

White Rose Research Online URL for this paper:  
<http://eprints.whiterose.ac.uk/42629/>

---

**Article:**

Khamas, S.K. (2010) A generalized asymptotic extraction solution for antennas in multilayered spherical media. *IEEE Transactions on Antennas and Propagation*, 58 (11). pp. 3743-3747. ISSN 0018-926X

<https://doi.org/10.1109/TAP.2010.2071371>

---

**Reuse**

Unless indicated otherwise, fulltext items are protected by copyright with all rights reserved. The copyright exception in section 29 of the Copyright, Designs and Patents Act 1988 allows the making of a single copy solely for the purpose of non-commercial research or private study within the limits of fair dealing. The publisher or other rights-holder may allow further reproduction and re-use of this version - refer to the White Rose Research Online record for this item. Where records identify the publisher as the copyright holder, users can verify any specific terms of use on the publisher's website.

**Takedown**

If you consider content in White Rose Research Online to be in breach of UK law, please notify us by emailing [eprints@whiterose.ac.uk](mailto:eprints@whiterose.ac.uk) including the URL of the record and the reason for the withdrawal request.



[eprints@whiterose.ac.uk](mailto:eprints@whiterose.ac.uk)  
<https://eprints.whiterose.ac.uk/>

## A Generalized Asymptotic Extraction Solution for Antennas in Multilayered Spherical Media

Salam K. Khamas

**Abstract**—An efficient model is developed to accelerate the convergence of the dyadic Green's function's (DGF) infinite summation when the source and observation points are placed in different layers of a dielectric sphere, thereby expediting computational analysis. The proposed procedure is based on asymptotic extraction principles in which the quasi-static images are extracted from the spectral domain DGF. The effectiveness of the approach is demonstrated in a method of moment model where a microstrip antenna as well as a conformal dipole array have been studied.

**Index Terms**—Dyadic Green's function, method of moments (MoM), spherical antennas.

### I. INTRODUCTION

Efficient computation of the dyadic Green's function for a multilayered dielectric sphere has been investigated in numerous research articles, where several approaches have been proposed to accelerate the convergence of the infinite series such as Watson or Shanks transformations [1]–[3], finite difference approximation [4], a large perfectly conducting (PEC) sphere consideration using Kummer's transformation [5], as well as incorporating the image theory of a planar structure in the solution [6]. Asymptotic extraction is a well-known procedure that has been extensively used for the efficient computation of the Sommerfeld type integrals in planar and cylindrical media [7], [8]. In a recent study [9], the asymptotic extraction approach has been introduced for spherical media, which has expedited the series convergence considerably when the field and observation points are located in the same layer. In many applications, the DGF needs to be computed when the field and source points are in different layers but still in the vicinity of each other. Examples include; patch antennas excited by a feed in a different layer, stacked arrays, three dimensional antennas, and volumetric arrays that penetrate a dielectric boundary.

In this article the asymptotic extraction introduced in [9] has been broadened to consider the problem of source and observation points positioned in different layers. The efficiency of the presented formulation has been confirmed by employing the proposed solution in a moment method model, where structures involve field and source points in adjacent layers have been studied. Two configurations have been considered including a probe-fed circular patch antenna, and a conformal dipole array.

### II. FORMULATION

For an antenna radiating next to a multilayered dielectric sphere, the DGF can be represented as a superposition of two components, the first,  $\bar{\mathbf{G}}_{0s}^{(fs)}$ , corresponds to radiation in an unbounded media and the second,  $\bar{\mathbf{G}}_{es}^{(fs)}$ , accounts for waves scattering owing to the presence of the sphere, i.e., [10]–[12]

$$\bar{\mathbf{G}}_e^{fs}(\mathbf{r}, \mathbf{r}') = \bar{\mathbf{G}}_{0s}^{(fs)}(\mathbf{r}, \mathbf{r}')\delta_s^s + \bar{\mathbf{G}}_{es}^{(fs)}(\mathbf{r}, \mathbf{r}') \quad (1)$$

Manuscript received February 12, 2010; revised April 21, 2010; accepted April 21, 2010. Date of publication September 02, 2010; date of current version November 03, 2010.

The author is with the Department of Electronic and Electrical Engineering, University of Sheffield, Sheffield S1 3JD, U.K. (e-mail: s.khamas@sheffield.ac.uk).

Color versions of one or more of the figures in this communication are available online at <http://ieeexplore.ieee.org>.

Digital Object Identifier 10.1109/TAP.2010.2071371

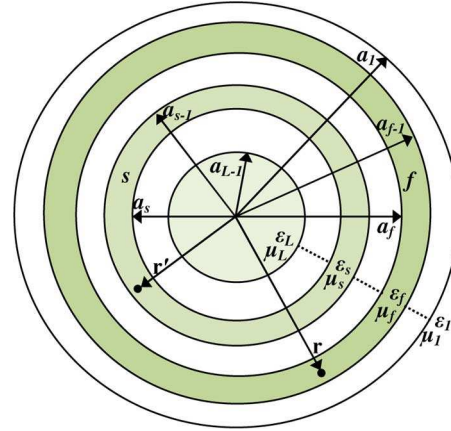


Fig. 1. A layered dielectric sphere.

where the superscript  $fs$  refers to the layers of field and source points,  $\mathbf{r}$  and  $\mathbf{r}'$ , respectively, and  $\delta_s^s$  is the Kronecker delta. It is well-known that  $\bar{\mathbf{G}}_{0s}^{(fs)}$  can be expressed in a closed form as [13]

$$\bar{\mathbf{G}}_{0s}^{(fs)}(\mathbf{r}, \mathbf{r}') = \left( \bar{\mathbf{I}} + \frac{1}{k_f^2} \nabla \nabla' \right) \frac{e^{-jk_f R}}{4\pi R} \quad (2)$$

whereas  $\bar{\mathbf{G}}_{es}^{(fs)}$  is represented as an infinite summation of spherical eigen modes as shown in the Appendix [12]. The summation can be truncated using a finite number of terms depending on the distance between the field and source points as well as other geometrical factors such as sphere radius and number of layers. When the field and source points are located in the same layer, then using (2) in conjunction with the asymptotic extraction approach [9] can enhance the computations of  $\bar{\mathbf{G}}_e^{fs}$  significantly. However, when the source and evaluation points are in different layers but in the proximity of each other, the computation efficiency of (1) degrades substantially as  $\bar{\mathbf{G}}_{0s}^{(fs)}$  is undefined and the asymptotic extraction is valid only for the source and field points within the same spherical layer. Therefore, a large number of summation terms must be added to accomplish convergence, which increases the computation time significantly and necessitates the computation of larger order Bessel and Hankel functions that may produce numerical under flows, or over flows. This article presents a methodology to enhance the computation efficiency of (1) when  $f \neq s$  using an asymptotic extraction technique, where the quasi-static images have been isolated from the infinite expansion.

#### A. Asymptotic Expansion Coefficients

Fig. 1 illustrates a spherical structure that consists of  $L$  layers, where each layer has a permittivity of  $\epsilon_i$  and a permeability of  $\mu_i$ , which has been assumed to be the same as that of free space, i.e.,  $\mu_0$ . When the source and field points are located in different layers, the asymptotic DGF can be attained by deriving expressions for the transmission and reflection coefficients when  $n \rightarrow \infty$ . This can be achieved by employing the large order spherical Bessel and Hankel functions principal asymptotic expressions [14], that is

$$j_n(kr) \approx \sqrt{\frac{1}{2kr(2n+1)}} \left( \frac{ekr}{2n+1} \right)^{n+\frac{1}{2}} \quad (3a)$$

$$h_n^{(2)}(kr) \approx j \sqrt{\frac{2}{kr(2n+1)}} \left( \frac{ekr}{2n+1} \right)^{-n-\frac{1}{2}} \quad (3b)$$

Following a procedure similar to that presented in [9], in which (3) is substituted in the reflection and transmission coefficients given by (18) in [12]. The resultant asymptotic expressions have then been substituted in the infinite series coefficients  $A_{M,N}^{f,s}$ ,  $B_{M,N}^{f,s}$ ,  $C_{M,N}^{f,s}$  and  $D_{M,N}^{f,s}$ . Therefore it can be shown that when  $f < s$  the following expansion coefficients contributions persist as  $n$  increases

$$C_N^{f<s} \sim T_{F_{s-1}}^V \Big|_a \cdots T_{F_f}^V \Big|_a \times \sum_{i=1}^{f-1} \frac{T_{F(f-1)}^V \Big|_a \cdots T_{F_i}^V \Big|_a}{T_{P(f-1)}^V \Big|_a \cdots T_{P_i}^V \Big|_a} R_{P_i}^V \Big|_a \quad (4)$$

$$A_N^{f<s} \sim T_{F_{s-1}}^V \Big|_a \cdots T_{F_f}^V \Big|_a \quad (5)$$

$$B_N^{f<s} \sim -T_{F_{s-1}}^V \Big|_a \cdots T_{F_f}^V \Big|_a \times \left( R_{F_s}^V \Big|_a + \sum_{i=s+1}^{L-1} \frac{T_{F(i-1)}^V \Big|_a \cdots T_{F_s}^V \Big|_a}{T_{P(i-1)}^V \Big|_a \cdots T_{P_s}^V \Big|_a} R_{F_i}^V \Big|_a \right) \quad (6)$$

whereas contributions of the other coefficients decline rapidly and asymptote to zero for larger  $n$ . In the above equations

$$T_{P_i}^V \sim -t_i \frac{j_n(k_{i+1}a_i)}{j_n(k_i a_i)}, \quad T_{F_i}^V \sim -t_i \frac{h_n^{(2)}(k_{i+1}a_i)}{h_n^{(2)}(k_i a_i)},$$

$$t_i = \frac{2\sqrt{\varepsilon_i \varepsilon_{i+1}}}{\varepsilon_{i+1} + \varepsilon_i}, \quad R_{P_i}^V \sim w_i \frac{h_n^{(2)}(k_i a_i)}{j_n(k_i a_i)},$$

$$R_{F_i}^V \sim w_i \frac{j_n(k_i a_i)}{h_n^{(2)}(k_i a_i)}, \quad w_i = \frac{\varepsilon_i - \varepsilon_{i+1}}{\varepsilon_i + \varepsilon_{i+1}}.$$

With the help of (3), it can be shown that when  $n \rightarrow \infty$ , the following relations can be attained

$$T_{F_{m-1}}^V \cdots T_{F_i}^V \sim -(-1)^{m-i} (t_{m-1} \cdots t_i) \left( \frac{k_i}{k_m} \right)^{n+1} \quad (7a)$$

$$T_{P_{m-1}}^V \cdots T_{P_i}^V \sim -(-1)^{m-i} (t_{m-1} \cdots t_i) \left( \frac{k_m}{k_i} \right)^n \quad (7b)$$

and

$$\left( \frac{k_i}{k_m} \right)^{n+1} h_n^{(2)}(k_i d) \sim h_n^{(2)}(k_m d) \quad (8a)$$

$$\left( \frac{k_m}{k_i} \right)^n j_n(k_i d) \sim j_n(k_m d). \quad (8b)$$

Substitution of (7)–(8) in (4)–(6) provides

$$C_N^{f<s} \sim -(-1)^{s-f} (t_{s-1} \cdots t_f) \sum_{i=1}^{f-1} w_i \frac{h_n^{(2)}(k_s a_i)}{j_n(k_f a_i)} \quad (9)$$

$$A_N^{f<s} \sim -(-1)^{s-f} (t_{s-1} \cdots t_f) \left( \frac{k_f}{k_s} \right)^{n+1} \quad (10)$$

$$B_N^{f<s} \sim (-1)^{s-f} (t_{s-1} \cdots t_f) \sum_{i=s}^{L-1} w_i \frac{j_n(k_s a_i)}{h_n^{(2)}(k_f a_i)}. \quad (11)$$

In these equations, the structure has been divided into three regions: the first corresponds to interfaces outer of the field layer, i.e.,  $i = 1 \rightarrow f - 1$ ; the second represents inner boundaries that are surrounded by the field and source layers, i.e.,  $i = f \rightarrow s - 1$ ; and the last accounts for interfaces of layers located between the source and the innermost layers, that is,  $i = s \rightarrow L - 1$ . Multiple reflections contributions are generally smaller than their local counterparts for larger  $n$  and decay rapidly as  $n$  increases; hence, they have been omitted.

Following a similar procedure, the required asymptotic expansion coefficients when  $f > s$  may be derived as

$$C_N^{f>s} \sim \frac{-(-1)^{f-s}}{t_{f-1} \cdots t_s} \sum_{i=1}^{s-1} w_i \frac{h_n^{(2)}(k_s a_i)}{j_n(k_f a_i)} \quad (12)$$

$$D_N^{f>s} \sim \frac{-(-1)^{f-s}}{t_{f-1} \cdots t_s} \left( \frac{k_s}{k_f} \right)^n \left( 1 - \sum_{i=s}^{f-1} w_i^2 \right) \quad (13)$$

$$B_N^{f>s} \sim \frac{(-1)^{f-s}}{t_{f-1} \cdots t_s} \sum_{i=f}^{L-1} w_i \frac{j_n(k_s a_i)}{h_n^{(2)}(k_f a_i)}. \quad (14)$$

### B. Asymptotic Dyadic Green's Functions

The asymptotic DGF components can be accomplished by substituting the coefficients of (9)–(11) in (22) to get

$$\begin{aligned} \bar{\mathbf{G}}_{es}^{(f<s)}(\mathbf{r}, \mathbf{r}') &\sim \frac{j(-1)^{s-f}}{4\pi k_f} \nabla \nabla' \sum_{n=0}^{\infty} (2n+1) P_n(\cos \gamma) \\ &\times (t_{s-1} \cdots t_f) \left\{ - \left( \frac{k_f}{k_s} \right)^{n+1} h_n^{(2)}(k_f r) j_n(k_s r') \right. \\ &- (1 - \delta_f^1) \sum_{i=1}^{f-1} w_i \frac{h_n^{(2)}(k_s a_i)}{j_n(k_f a_i)} j_n(k_f r) j_n(k_s r') \\ &\left. + \left( 1 - \delta_s^L \right) \sum_{i=s}^{L-1} w_i \frac{j_n(k_s a_i)}{h_n^{(2)}(k_f a_i)} h_n^{(2)}(k_f r') h_n^{(2)}(k_s r) \right\} \quad (15) \end{aligned}$$

where,  $P_n(\cos \gamma)$  is the Legendre polynomial of degree  $n$ , and  $\cos \gamma = \cos \theta \cos \theta' + \sin \theta \sin \theta' \cos(\phi - \phi')$ . It should be noted that the addition theorem of Legendre polynomial has been used to reduce the double summations of (22) to a single summation [15]. Furthermore, the vector operator  $\nabla \nabla'$  has been introduced to develop a unified asymptotic DGF expression as described in [9].

With the help of (3), (8), (15) may be expressed as

$$\begin{aligned} \bar{\mathbf{G}}_{es}^{(f<s)}(\mathbf{r}, \mathbf{r}') &\sim \frac{j(-1)^{s-f}}{4\pi k_f} \nabla \nabla' \sum_{n=0}^{\infty} (2n+1) P_n(\cos \gamma) \\ &\times (t_{s-1} \cdots t_f) \left\{ -h_n^{(2)}(k_s r) j_n(k_s r') \right. \\ &- (1 - \delta_f^1) \sum_{i=1}^{f-1} w_i \left( \frac{a_i}{r} \right) h_n^{(2)}(k_s d_i) j_n(k_s r') \\ &\left. + \left( 1 - \delta_s^L \right) \sum_{i=s}^{L-1} w_i \left( \frac{a_i}{r} \right) j_n(k_s d_i) h_n^{(2)}(k_s r') \right\} \quad (16) \end{aligned}$$

in which  $d_i = (a_i^2)/r$ . In the first term of (16), waves traveling between the upper boundary of the field layer and the lower boundary of the source layer have been represented as waves traveling in an unbounded media that has a propagation constant of  $k_s$ . Such waves have then been weighted by the corresponding transmission coefficients to take account of the existence of inner interfaces that are surrounded by the source and field layers. Reflections of these waves at dielectric boundaries exterior to the aforementioned layers, i.e., when  $i \leq f - 1$  or  $i \geq s$ , have been incorporated in the model using the second and the third terms of (16).

Similarly, it can be shown that

$$\begin{aligned} \bar{\mathbf{G}}_{es}^{(f>s)}(\mathbf{r}, \mathbf{r}') &\sim \frac{j(-1)^{s-f}}{4\pi k_f} \nabla \nabla' \sum_{n=0}^{\infty} (2n+1) P_n(\cos \gamma) \\ &\times \frac{1}{t_{f-1} \cdots t_s} \left\{ - \left( 1 - \sum_{i=s}^{f-1} w_i^2 \right) j_n(k_s r) h_n^{(2)}(k_s r') \right. \\ &- (1 - \delta_s^1) \sum_{i=1}^{s-1} w_i \left( \frac{a_i}{r} \right) h_n^{(2)}(k_s d_i) j_n(k_s r') \\ &\left. + \left( 1 - \delta_f^L \right) \sum_{i=f}^{L-1} w_i \left( \frac{a_i}{r} \right) j_n(k_s d_i) h_n^{(2)}(k_s r') \right\}. \quad (17) \end{aligned}$$

A unified expression of (16), (17), which is also valid when  $f = s$ , can be attained as

$$\begin{aligned} \bar{\mathbf{G}}_{e_s}^{(fs)}(\mathbf{r}, \mathbf{r}')_{n \rightarrow \infty} &\sim \frac{-j(-1)^{s-f} T}{4\pi k_f} \\ &\times \nabla \nabla' \sum_{n=0}^{\infty} (2n+1) P_n(\cos \gamma) \\ &\times \left\{ \gamma j_n(k_s r) h_n^{(2)}(k_s r') \right. \\ &+ (1 - \delta_{m_1}^1) \sum_{i=1}^{m_1-1} w_i \left( \frac{a_i}{r} \right) h_n^{(2)}(k_s d_i) j_n(k_s r') \\ &\left. - \left( 1 - \delta_{m_2}^L \right) \sum_{i=m_2}^{L-1} w_i \left( \frac{a_i}{r} \right) j_n(k_s d_i) h_n^{(2)}(k_s r') \right\} \quad (18) \end{aligned}$$

in which  $m_1 = \min(f, s)$ ,  $m_2 = \max(f, s)$ , and

$$\gamma = 1, \quad T = t_{s-1} \cdots t_f \quad f < s \quad (19a)$$

$$\gamma = 0, \quad T = 1 \quad f = s \quad (19b)$$

$$\gamma = 1 - \sum_{i=s}^{f-1} w_i^2, \quad T = \frac{1}{t_{f-1} \cdots t_s} \quad f > s. \quad (19c)$$

Closed-form representation of (18) can be accomplished by employing the addition theorem of the spherical Hankel function [15] as

$$\begin{aligned} \bar{\mathbf{G}}_{n \rightarrow \infty}^{(fs)} &\sim \frac{(-1)^{s-f}}{4\pi k_f k_s} T \nabla \nabla' \left\{ \gamma \frac{e^{-jk_s R}}{R} \right. \\ &+ \left( (1 - \delta_{m_1}^1) \sum_{i=1}^{m_1-1} - (1 - \delta_{m_2}^L) \sum_{i=m_2}^{L-1} \right) \\ &\left. \times w_i \left( \frac{a_i}{r} \right) \frac{e^{-jk_s R_i}}{R_i} \right\} \quad (20) \end{aligned}$$

where the separation distances are given by  $R = \sqrt{r'^2 + r^2 - 2r'r \cos \gamma}$ , and  $R_i = \sqrt{r'^2 + d_i^2 - 2r'd_i \cos \gamma}$ .

Therefore, a generalized and computationally efficient representation of (1) can be achieved as

$$\begin{aligned} \bar{\mathbf{G}}_e^{fs}(\mathbf{r}, \mathbf{r}') &= \bar{\mathbf{G}}_{0_s}^{(fs)}(\mathbf{r}, \mathbf{r}') \delta_f^s + \bar{\mathbf{G}}_{n \rightarrow \infty}^{(fs)} \\ &+ \left\{ \bar{\mathbf{G}}_{e_s}^{(fs)}(\mathbf{r}, \mathbf{r}') - \bar{\mathbf{G}}_{e_s}^{(fs)}(\mathbf{r}, \mathbf{r}')_{n \rightarrow \infty} \right\} \quad (21) \end{aligned}$$

where  $\bar{\mathbf{G}}_{n \rightarrow \infty}^{(fs)}$  and  $\bar{\mathbf{G}}_{e_s}^{(fs)}(\mathbf{r}, \mathbf{r}')_{n \rightarrow \infty}$  are given by (20) and (18), respectively.

### III. RESULTS

The developed expressions have been employed in a MoM model, where four-layer geometry has been considered. The first layer has been assumed to be a free space, the second is a spherical superstrate that has a permittivity of  $\epsilon_2$ , the third is a spherical substrate with a permittivity of  $\epsilon_3$ , and the innermost layer is a PEC spherical core.

A probe-fed circular patch antenna with a radius of 1.88 cm has been modeled using substrate and superstrate thicknesses of 0.32 cm and relative permittivities of  $\epsilon_{r3} = 2.47$  and  $\epsilon_{r2} = 5$ . A PEC spherical core radius of 5 cm has been chosen. The feeding probe is placed in the spherical substrate and connected at its lower end to the PEC core and to the patch antenna at the other end. The configuration has been modeled twice: first assuming the conformal patch is printed on the substrate side of the interface, and then assuming the patch is printed on the superstrate side of the interface. In the former case, the patch and the

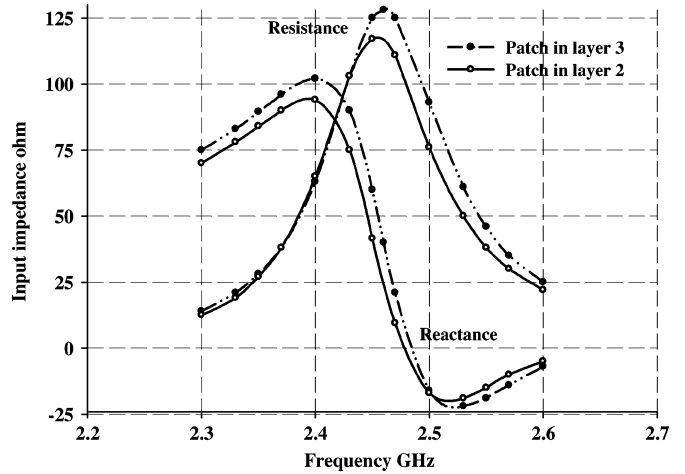


Fig. 2. Input impedance of a spherical circular patch antenna placed on the interface between layers 2 and 3 and fed by a probe located in layer 3.

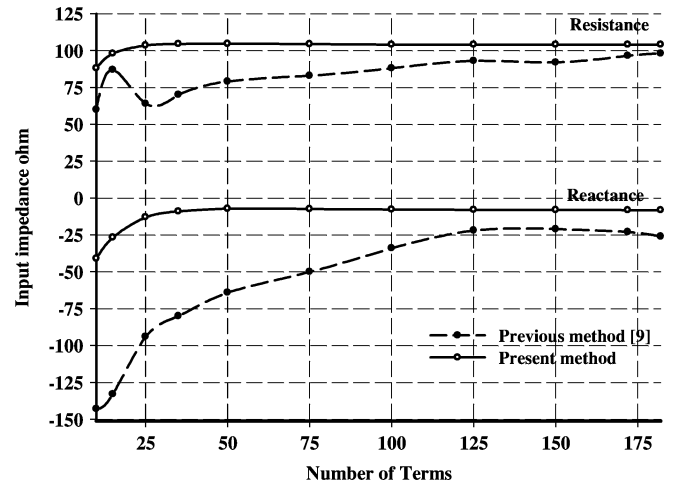


Fig. 3. Convergence of the input impedance of a spherical patch located at the superstrate side of an interface and fed by a probe positioned at the adjacent substrate.

probe are located in the same layer, while in the latter they are placed in different layers. Fig. 2 illustrates the computed input impedances for the aforementioned cases. As expected, the same results have been obtained regardless of what side of the interface is the patch located at, which validates the presented formulation. The slight discrepancy between the two sets of results can be explained as a result of numerical computations of Hankel functions using different arguments. The convergence of the input impedance at 2.47 GHz is demonstrated in Fig. 3 when the patch and the probe are in different layers, where it can be observed that the proposed model provides convergence using 40 summation terms. This is to be compared to more than 180 terms when the asymptotic extraction is applied only for source and field points that are located in the same layer.

As another example, an array of two  $\phi$ -directed half-wavelength center-fed dipoles is considered. The structure consists of a PEC spherical core with a radius of  $1.5\lambda_0$  that is covered by a substrate with  $\epsilon_{r3} = 2.5$  and a thickness of  $0.1\lambda_0$ . The spherical superstrate relative permittivity has been chosen as  $\epsilon_{r2} = 1$ , and the dipoles centers are separated by an arc distance of  $d$ . The correctness of the formulation has been validated by comparing the mutual impedance between the

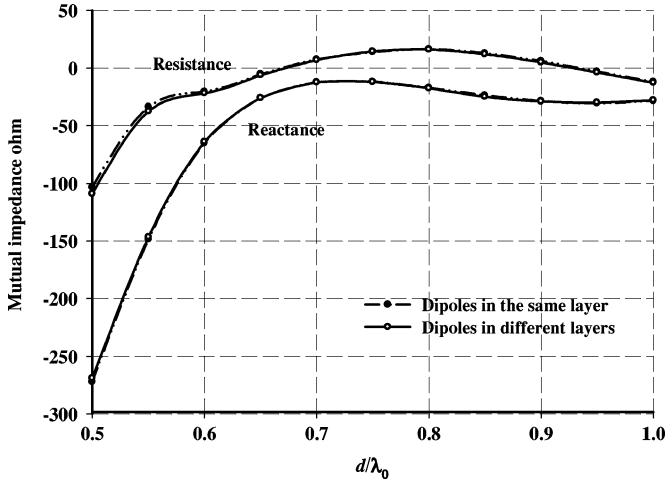


Fig. 4. Mutual impedance between two conformal  $0.5\lambda_0$  dipole printed on grounded spherical substrate with  $\epsilon_{r3} = 2.5$  and a PEC core radius of  $1.5\lambda_0$ .

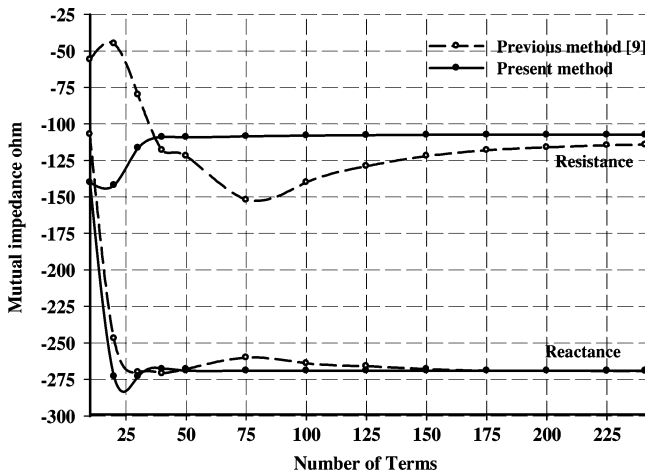


Fig. 5. Convergence of the mutual impedance between conformal dipoles printed on opposite sides of a spherical interface when their centres are separated by an arc distance of  $d = 0.5\lambda_0$ .

dipoles when they are both printed at the same side of the dielectric interface to that when each is printed at a different side of the same interface. Fig. 4 presents the mutual impedance when the dipoles are placed on the interface of the second and the third layers. As expected, the results are identical irrespective of whether the conformal dipoles are printed on the same side or opposite sides of the interface. Fig. 5 illustrates the convergence of the mutual impedance for dipoles printed on opposite sides of a dielectric boundary, where the present and the previous [9] methods are compared. The advantage of the present formulation is evident as the convergence has been accelerated significantly when the asymptotic extraction is applied in computing the coupling between the source and field points that are located in different layers.

#### IV. CONCLUSION

The asymptotic extraction for antennas in a spherical media [9] has been extended to consider the problem of a source and an observation points that are positioned in different layers. As a result, an efficient solution has been developed by isolating the quasi-static images from the infinite summation. The effectiveness and correctness of the presented method have been confirmed using a moment method model, where input and mutual impedances have been computed for various structures. The convergence speed has been accelerated by several folds when the proposed model is adopted, which improves the computation

efficiency significantly. The presented formulation is unified, hence it can be used in the analysis of arbitrarily located source and field points, i.e., when  $f \neq s$  as well as when  $f = s$ .

#### APPENDIX

The DGF component,  $\bar{\mathbf{G}}_{es}^{(fs)}$ , is given by [12]

$$\begin{aligned} \bar{\mathbf{G}}_{es}^{(fs)}(\mathbf{r}, \mathbf{r}') &= \frac{jk_s}{4\pi} \sum_{n=0}^{\infty} \sum_{m=0}^n (2 - \delta_m^0) \\ &\times \frac{2n+1}{n(n+1)} \frac{(n-m)!}{(n+m)!} \\ &\times \left\{ \Delta_1 \mathbf{M}_{mn}^{(2)}(k_f) \left( \Delta_2 A_M^{fs} \mathbf{M}'_{mn}(k_s) \right. \right. \\ &+ \Delta_3 B_M^{fs} \mathbf{M}'_{mn}{}^{(2)}(k_s) \Big) \\ &+ \Delta_1 \mathbf{N}_{mn}^{(2)}(k_f) \left( \Delta_2 A_N^{fs} \mathbf{N}'_{mn}(k_s) \right. \\ &+ \Delta_3 B_N^{fs} \mathbf{N}'_{mn}{}^{(2)}(k_s) \Big) \\ &+ \Delta_4 \mathbf{M}_{mn}(k_f) \left( \Delta_2 C_M^{fs} \mathbf{M}'_{mn}(k_s) \right. \\ &+ \Delta_3 D_M^{fs} \mathbf{M}'_{mn}{}^{(2)}(k_s) \Big) \\ &+ \Delta_4 \mathbf{N}_{mn}(k_f) \left( \Delta_2 C_N^{fs} \mathbf{N}'_{mn}(k_s) \right. \\ &\left. \left. + \Delta_3 D_N^{fs} \mathbf{N}'_{mn}{}^{(2)}(k_s) \right) \right\} \end{aligned} \quad (22)$$

where  $\mathbf{M}_{mn}$  and  $\mathbf{N}_{mn}$  are the well-known spherical vector eigen-functions of the transverse electric,  $\text{TE}_{mn}$ , and transverse magnetic,  $\text{TM}_{mn}$ , modes, respectively, the superscript (2) refers to the second type spherical Hankel functions,  $\Delta_1 = (1 - \delta_f^L)$ ,  $\Delta_2 = (1 - \delta_s^L)$ ,  $\Delta_3 = (1 - \delta_s^L)$ , and  $\Delta_4 = (1 - \delta_f^L)$ . Explicit expressions for the scattering DGF coefficients  $A_{M,N}^{fs}$ ,  $B_{M,N}^{fs}$ ,  $C_{M,N}^{fs}$  and  $D_{M,N}^{fs}$  are reported in [12].

#### REFERENCES

- [1] G. M. Watson, "The diffraction of electric waves by the earth," *Proc. Royal Society*, vol. 95, pp. 83–99, 1919.
- [2] D. Shanks, "Non-linear transformation of divergent and slowly convergent sequences," *J. Math. Phys.*, vol. 34, pp. 1–42, 1955.
- [3] F. M. Tesche, A. R. Neureuther, and R. E. Stovall, "The analysis of monopole antennas located on a spherical vehicle: Part 2, numerical and experimental results," *IEEE Trans. Electromagn. Compat.*, vol. 18, pp. 8–15, Feb. 1976.
- [4] V. I. Okhmatovski and A. C. Cangellaris, "Efficient calculation of the electromagnetic dyadic Green's function in spherical layered media," *IEEE Trans. Antennas Propag.*, vol. 51, pp. 3209–3220, 2003.
- [5] L. W. Li, T. Fei, Q. Wu, and T. S. Yeo, "Convergence acceleration for calculating radiated fields by a vertical electric dipole in the presence of a large sphere," in *IProc. IEEE Antennas Propag. Soc. Int. Symp.*, July 2005, vol. 2B, pp. 117–120.
- [6] B. D. Milovanovic, "Numerical analysis of radial thin-wire antenna in presence of conducting sphere," *Elect. Lett.*, vol. 16, no. 15, pp. 611–612, Jul. 1980.
- [7] D. R. Jackson and N. G. Alexopoulos, "An asymptotic extraction technique for evaluating sommerfeld-type integrals," *IEEE Trans. Antennas Propag.*, vol. 34, pp. 1467–1470, Dec. 1986.
- [8] J. Sun, C. F. Wang, L. W. Li, and M. S. Leong, "Further improvement for fast computation of mixed potential Green's functions for cylindrically stratified media," *IEEE Trans. Antennas Propag.*, vol. 52, pp. 3026–3036, Nov. 2004.
- [9] S. K. Khamas, "Asymptotic extraction approach for antennas in a multilayered spherical media," *IEEE Trans. Antennas Propag.*, vol. 58, no. 3, pp. 1003–1008, Mar. 2010.
- [10] C. T. Tai, *Dyadic Green's Functions in Electromagnetics Theory*. Scranton, PA: Intext educational, 1971.
- [11] W. C. Chew, *Waves and Fields in Inhomogeneous Media*. New York: Van Nostrand, 1990.
- [12] L. W. Li, P. S. Kooi, M. S. Leong, and T. S. Yeo, "Electromagnetic dyadic Green's function in spherically multilayered media," *IEEE Trans. Microwave Theory Tech.*, vol. 42, pp. 2302–2310, Dec. 1994.

- [13] K. W. Leung, K. M. Luk, K. Y. A. Lai, and D. Lin, "Theory and experiment of a coaxial probe fed hemispherical dielectric resonator antenna," *IEEE Trans. Antennas Propag.*, vol. 41, pp. 1390–1398, 1993.
- [14] M. Abramowitz and I. A. Stegun, *Handbook of Mathematical Functions With Formulas, Graphs, and Mathematical Tables*. Washington, DC: Government Printing Office, 1964.
- [15] R. F. Harrington, *Time Harmonic Electromagnetic Fields*. New York: McGraw-Hill, 1961.

## Lack of Rotation Invariance in Short-Pulse Communication Between Broadband Circular-Polarization Antennas

H. D. Foltz, J. S. McLean, A. Medina, and J. H. Alvarez Jerkov

**Abstract**—There are many antenna designs capable of producing high quality circular polarization over very wide bandwidth. One of the beneficial attributes of circular polarization seen in narrowband applications is that one or both of the antennas in a link can be rotated around the boresight direction without significantly affecting the received signal. However, this does not apply to a broadband system, in which the received pulse shape will change under rotation. Calculations of maximum possible correlation between the rotated and unrotated pulse shapes as the antenna is rotated are presented, along with an experimental example. It is also shown that in general it is not possible to have the pulse shape and amplitude invariant under rotation for a broadband signal, even if completely general polarizations and antenna transfer functions are allowed.

**Index Terms**—Circular polarization, pulse antennas, ultra-wideband.

### I. INTRODUCTION

Perfect circular polarization requires that the two orthogonal components of the radiated electric fields be in quadrature at all frequencies. This also applies to the components of the vector effective length [1], [2], or equivalently, the vector antenna transfer function [3]–[6] since the radiated field is proportional to both of these quantities. In particular

$$\begin{aligned} \mathbf{E}(\omega; R, \theta, \phi) &= -j\omega\sqrt{\eta_0}\mathbf{H}(\omega; \theta, \phi)\frac{e^{-j\beta R}}{2\pi Rc_0}A(\omega) \\ &= -j\omega\frac{\eta_0\sqrt{Z_0}}{Z_0 + Z_A(\omega)}\mathbf{h}_{\text{eff}}(\omega; \theta, \phi)\frac{e^{-j\beta R}}{2\pi Rc_0}A(\omega) \quad (1) \end{aligned}$$

where  $\mathbf{H}$  is the vector antenna transfer function,  $Z_A$  is the antenna input impedance, and  $\mathbf{h}_{\text{eff}}$  is the antenna effective length. Neither  $\mathbf{H}$  nor  $\mathbf{h}_{\text{eff}}$  have  $R$  dependence since the far field is assumed. The quantity  $A(\omega) = V^+(\omega)/\sqrt{(Z_0)}$  is the normalized incident wave at the

Manuscript received July 02, 2009; revised February 27, 2010; accepted March 29, 2010. Date of publication August 30, 2010; date of current version November 03, 2010. This work was supported in part by the U.S. Army Research Office under Grant W911NF-06-1-0420 and in part by an NSF MRI Grant 0421352.

H. D. Foltz and J. H. Alvarez Jerkov are with the Department of Electrical Engineering, University of Texas - Pan American, Edinburg, TX 78539 USA (e-mail: hfoltz@panam.edu).

J. S. McLean and A. Medina are with the TDK RF Solutions, Inc., Cedar Park, TX 78613 USA.

Color versions of one or more of the figures in this communication are available online at <http://ieeexplore.ieee.org>.

Digital Object Identifier 10.1109/TAP.2010.2071344

input to the antenna. If the vector antenna transfer function is defined in spherical coordinates as

$$\mathbf{H}(\omega; \theta, \phi) = H_\theta(\omega; \theta, \phi)\mathbf{a}_\theta + H_\phi(\omega; \theta, \phi)\mathbf{a}_\phi \quad (2)$$

then for right hand circular polarization (RHCP) at all frequencies we need

$$H_\theta(\omega; \theta, \phi) = j \operatorname{sgn}(\omega)H_\phi(\omega; \theta, \phi) \quad (3)$$

and for LHCP at all frequencies we need

$$H_\phi(\omega; \theta, \phi) = j \operatorname{sgn}(\omega)H_\theta(\omega; \theta, \phi). \quad (4)$$

A recent comprehensive analysis of the time domain behavior of circular polarization antennas was published by Shlivinski [7], in which it is pointed out that multiplication by  $j \operatorname{sgn}(\omega)$  in the frequency domain is equivalent to Hilbert transformation in the time domain. Therefore, in the case of true broadband circular polarization, the components of the antenna impulse response  $h_\theta(t; \theta, \phi) = \mathcal{F}^{-1}\{H_\theta(\omega; \theta, \phi)\}$  and  $h_\phi(t; \theta, \phi) = \mathcal{F}^{-1}\{H_\phi(\omega; \theta, \phi)\}$  form a Hilbert transform pair. This is independent of whether the other characteristics of the antenna, such as the pattern or input impedance, are broadband. The Hilbert relationship also applies to the components of the electric field, regardless of the form of the input signal  $A(\omega)$ .

One of the attractive features of circular polarization in narrowband applications is rotational invariance, specifically, the ability to rotate either the transmit or receive antenna about the boresight direction without significantly changing the received signal. This applies to cases where one or both of the antennas are circularly polarized. In the narrowband case the signal can be represented by a bandpass model; for example, if the  $\phi$  component of the electric field in a particular direction is modeled by

$$E_\phi(t) = m(t)\cos(\omega_0 t) \quad (5)$$

then for a RHCP antenna the  $\theta$  component will be given by

$$E_\theta(t) = -m(t)\sin(\omega_0 t) \quad (6)$$

the key assumption being that the baseband signal  $m(t)$  has a bandwidth that is small compared to the carrier frequency  $\omega_0$ . Many narrowband communication systems are not sensitive to the absolute value of the carrier phase, and thus the change from cosine to sine in the carrier is irrelevant. In a broadband system this assumption no longer holds.

### II. CHANGE OF PORT-TO-PORT TRANSFER FUNCTION UNDER ROTATION

To simplify the analysis we initially assume communication between two antennas capable of perfect RHCP over their operating bandwidth, located along the  $z$ -axis, with the direction of propagation in the  $+z$ -direction, as shown in Fig. 1(a). The transmit antenna polarization is:

$$\mathbf{H}_T(\omega) = \frac{1}{\sqrt{2}}H_T(\omega)(j \operatorname{sgn}(\omega)\mathbf{a}_x + \mathbf{a}_y). \quad (7)$$

The receive antenna polarization is

$$\mathbf{H}_R(\omega) = \frac{1}{\sqrt{2}}H_R(\omega)(-j \operatorname{sgn}(\omega)\mathbf{a}_x + \mathbf{a}_y). \quad (8)$$

The direction of the  $x$ -component is reversed because the receive antenna is rotated about the  $y$ -axis to face the transmit antenna. The port-to-port transfer function  $S_{21}(\omega)$  can be written in general as

$$S_{21}(\omega) = j\omega\mathbf{H}_T(\omega) \cdot \mathbf{H}_R(\omega)\frac{e^{-j\beta d}}{2\pi dc_0} \quad (9)$$